NeuroImage 68 (2013) 248–262

Contents lists available at SciVerse ScienceDirect

NeuroImage

journal homepage: www.elsevier.com/locate/ynimg

Mapping interictal epileptic discharges using mutual information between concurrent EEG and fMRI

César Caballero-Gaudes [a,e,*], Dimitri Van de Ville [a,d], Frédéric Grouiller [a,c], Rachel Thornton [f,g], Louis Lemieux [f,g], Margitta Seeck [b], François Lazeyras [a], Serge Vulliemoz [b,c]

[a] Department of Radiology and Medical Informatics, University of Geneva, Geneva, Switzerland
[b] Presurgical Epilepsy Evaluation Unit, Neurology Department, University Hospital of Geneva, Geneva, Switzerland
[c] Functional Brain Mapping Laboratory, University of Geneva, Geneva, Switzerland
[d] Medical Image Processing Lab, Institute of Bioengineering, Ecole Polytechnique Fédérale de Lausanne, Lausanne, Switzerland
[e] Basque Center on Cognition, Brain and Language, Donostia, Spain
[f] Department of Clinical and Experimental Epilepsy, UCL, Institute of Neurology, Queen Square, WC1N 3BG, London, United Kingdom
[g] Epilepsy Society, MRI Unit, Chalfont St. Peter, Buckinghamshire, SL9 0RJ, United Kingdom

ARTICLE INFO

Article history:
Accepted 7 December 2012
Available online 14 December 2012

Keywords:
Mutual information
BOLD
EEG–fMRI
Epilepsy
Interictal discharges

ABSTRACT

Objective: The mapping of haemodynamic changes related to interictal epileptic discharges (IED) in simultaneous electroencephalography (EEG) and functional MRI (fMRI) studies is usually carried out by means of EEG-correlated fMRI analyses where the EEG information specifies the model to test on the fMRI signal. The sensitivity and specificity critically depend on the accuracy of EEG detection and the validity of the haemodynamic model. In this study we investigated whether an information theoretic analysis based on the mutual information (MI) between the presence of epileptic activity on EEG and the fMRI data can provide further insights into the haemodynamic changes related to interictal epileptic activity. The important features of MI are that: 1) both recording modalities are treated symmetrically; 2) no requirement for a-priori models for the haemodynamic response function, or assumption of a linear relationship between the spiking activity and BOLD responses, and 3) no parametric model for the type of noise or its probability distribution is necessary for the computation of MI.
Methods: Fourteen patients with pharmaco-resistant focal epilepsy underwent EEG–fMRI and intracranial EEG and/or surgical resection with positive postoperative outcome (seizure freedom or considerable reduction in seizure frequency) was available in 7/14 patients. We used nonparametric statistical assessment of the MI maps based on a four-dimensional wavelet packet resampling method. The results of MI were compared to the statistical parametric maps obtained with two conventional General Linear Model (GLM) analyses based on the informed basis set (canonical HRF and its temporal and dispersion derivatives) and the Finite Impulse Response (FIR) models.
Results: The MI results were concordant with the electro-clinically or surgically defined epileptogenic area in 8/14 patients and showed the same degree of concordance as the results obtained with the GLM-based methods in 12 patients (7 concordant and 5 discordant). In one patient, the information theoretic analysis improved the delineation of the irritative zone compared with the GLM-based methods.
Discussion: Our findings suggest that an information theoretic analysis can provide clinically relevant information about the BOLD signal changes associated with the generation and propagation of interictal epileptic discharges. The concordance between the MI, GLM and FIR maps support the validity of the assumptions adopted in GLM-based analyses of interictal epileptic activity with EEG–fMRI in such a manner that they do not significantly constrain the localization of the epileptogenic zone.

Introduction

Simultaneous functional magnetic resonance imaging (fMRI) and electroencephalography (EEG) is a powerful multimodal technique to map brain regions involved in interictal epileptic networks in patients with refractory focal epilepsy (Bénar et al., 2006; Gotman, 2008; Gotman and Pittau, 2011; Lazeyras et al., 2000; Vulliemoz et al., 2010a). Mapping the haemodynamic changes related to interictal epileptic discharges (IED) can help to non-invasively localize the focus of epileptic seizures, which has important clinical relevance for targeting implantation of intracranial EEG (icEEG) electrodes given the high spatial resolution and whole-brain coverage of blood oxygenation level-dependent (BOLD) fMRI data (Zijlmans et al., 2007).

Most methods aimed at mapping haemodynamic changes associated with IED based on simultaneous EEG–fMRI acquisition rely on the identification of IED on the EEG by expert observers and the timing of the EEG

* Corresponding author at: Basque Center on Cognition, Brain and Language, Paseo Mikeletegi 69, 2nd floor, 20009 Donostia, Spain. Fax: +34 943 309 052.
E-mail address: c.caballero@bcbl.eu (C. Caballero-Gaudes).

1053-8119/$ – see front matter © 2012 Elsevier Inc. All rights reserved.
http://dx.doi.org/10.1016/j.neuroimage.2012.12.011

events is used to define a model predicting the fMRI time series through convolution with a haemodynamic model. The sensitivity and specificity of the localization of the epileptogenic focus critically depend on the accuracy and validity of the General Linear Model (GLM) describing the haemodynamic changes related to the epileptic events. In general, a particular shape of the haemodynamic response function (HRF) is assumed, such as the canonical HRF, and a large number of studies have demonstrated the usefulness of this approach to detect IED-related BOLD activity (Bénar et al., 2002; Gotman, 2008; Gotman and Pittau, 2011; Grouiller et al., 2011; Hamandi et al., 2006; Thornton et al., 2010a,b, 2011; Vulliemoz et al., 2009). Nevertheless, in some patients with epilepsy, the shape of the HRF may significantly deviate from the canonical HRF to an external stimulus in healthy adults (Grouiller et al., 2010; Jacobs et al., 2007, 2008; Lemieux et al., 2008; Salek-Haddadi et al., 2006), which can considerably decrease the sensitivity of the analysis. Several approaches have been used to deal with variability in the HRF: a) incorporating additional basis functions such as the temporal derivative and the dispersion derivatives of the canonical HRF (Salek-Haddadi et al., 2006); b) adopting a model for the HRF with no shape constraints such as the finite impulse response (FIR) (Lu et al., 2006, 2007; van Houdt et al., 2010a); c) considering Fourier sets (Lemieux et al., 2008); and d) introducing multiple HRF shapes with successive latencies (Bagshaw et al., 2004). As opposed to model-based approaches, exploratory data-driven techniques of fMRI analysis, such as independent component analysis (ICA) (Iriarte et al., 2006; Jann et al., 2008; LeVan et al., 2010a,b; Marques et al., 2009; Moeller et al., 2011; Rodionov et al., 2007; Thornton et al., 2010a) or temporal clustering analysis (TCA) (Hamandi et al., 2005; Khatamian et al., 2011; Morgan et al., 2004, 2008), have shown their ability to capture BOLD signal changes without imposing constraints on the HRF shape. However, these methods normally analyze the fMRI data without link to the information contained in the EEG data. A spatial topography-based analysis has also shown substantial improvements in the sensitivity of EEG–fMRI analysis (Grouiller et al., 2011) when IED-related events are not evident (or not in a sufficient number) in the scalp EEG during the fMRI session. Alternatively, "paradigm free mapping" is another promising technique that enables model-based haemodynamic deconvolution with no prior knowledge about the timing of the events. This recent methodology has been proposed for the study of epilepsy with simultaneous EEG–fMRI based on a dictionary of "haemodynamic atoms" (Caballero-Gaudes, 2010; Caballero-Gaudes et al., in press) and based on a multiscale haemodynamic-tailored wavelet decomposition (Khalidov et al., 2011; Lopes et al., 2012).

Here we investigate an information theoretic approach (Cover and Thomas, 1991; Shannon, 1948) for the study of IED-related BOLD signal changes with concurrent EEG–fMRI. Information theoretic approaches have been already applied to integrate EEG and fMRI BOLD data in sensory and cognitive tasks (Ostwald et al., 2010, 2011, 2012), and spontaneous brain activity in early visual cortices of anaesthetized monkeys (Magri et al., 2012), as well as measuring functional connectivity with transfer entropy in a visuo-motor tracking task (Lizier et al., 2010). In this work, we aimed to demonstrate that the mutual information (MI) between an EEG score reflecting IED activity and the fMRI data can serve as an alternative measure to explore IED-related haemodynamic activity and indirectly evaluate the influence of the assumptions associated with GLM-based analyses. The most prominent feature of this information theoretic approach is that it balances the information obtained with both imaging modalities (Fuhrmann Alpert et al., 2007; Panzeri et al., 2008) since the MI is a symmetric metric and no signal dominates the other in contrast to EEG-based modeling of the fMRI signal. Besides, it is a generalization of the concept of correlation between two variables as it includes all contributions of higher-order correlations (Hlinka et al., 2011; Panzeri et al., 2008). Therefore, it does not assume a linear relationship between the signals as in conventional linear regression analysis and it can be applied to investigate nonlinear relationships (Ostwald and Bagshaw, 2011; Panzeri et al., 2008). In addition, it does not require a-priori models for the HRF shape nor does it assume a linear relationship between the spiking activity detected on the EEG and the BOLD responses (Magri et al., 2012). Since it relies on the nonparametric estimation of probability density functions, it requires no parametric model regarding the effect of noise (e.g., additive or multiplicative) or its probability distribution, typically assumed as Gaussian in order to obtain statistical inference with T- or F-statistics. Furthermore, our approach used nonparametric statistical assessment of the MI statistics based on a 4D spatio-temporal wavelet resampling approach (Patel et al., 2006).

The analysis was applied to data from 14 patients with pharmacoresistant focal epilepsy and its performance was evaluated by comparing our results with the estimated localization of the epileptic focus based on electro-clinical and radiological presentation and, when available, to invasive EEG and/or resection area in post-operatively seizure-free patients. Furthermore, we compared our approach with two types of GLM-based mapping: using the informed basis set with the canonical HRF plus its temporal and dispersion derivatives (i.e. assuming a particular shape of the HRF) or a Finite Impulse Response (FIR) model (i.e. with no particular assumption on the shape of the HRF), and where both models assume linearity in the neurovascular coupling of the BOLD response and gaussianity of the model residuals.

Materials and methods

Patients and electro-clinical details

We tested our information-theoretic approach in 14 patients with refractory focal epilepsy from the EEG–fMRI databases of the Neurology Department of Geneva University Hospital (Geneva, Switzerland) and the UCL Institute of Neurology and Epilepsy Society (London, United Kingdom). In order to test our analysis strategy, we selected patients with frequent IED. Clinical details and electrophysiological data of the patients are described in Table 1. Five patients underwent intracranial EEG (icEEG) examination, and six patients had surgical resection. The EEG–fMRI procedures were approved by the local ethical committee and all patients and the parents of pediatric patients gave written informed consent.

EEG–fMRI acquisition and data preprocessing

All patients were scanned on 3 T MRI scanners (Geneva: Siemens Magnetom Trio equipped with a 12-channel head receive coil and body transmit coil; London: Signa Excite HDX, GE Medical Systems) where they were asked to remain at rest with the eyes closed during the acquisition. A 32, 64 or 96-electrode MR-compatible EEG cap (EasyCaps, FalkMinnow Services) was used to obtain the EEG recordings according to the 10–20 or 10–10 electrode position convention. Electrodes were equipped with an additional 5 kΩ resistance and impedances were kept as low as possible. EEG was acquired at 5000 Hz using 1–3 MR-compatible amplifiers (Brain Products, Munich, Germany) and was synchronized with the MR clock. EEG recordings were corrected for gradient and pulse-related artifacts using average subtraction methods (Allen et al., 1998, 2000) implemented in Vision Analyzer (Brain Products, Munich, Germany). If residual artifacts were observed, the EEG data was also decomposed with temporal independent component analysis using the Infomax algorithm (Bell and Sejnowski, 1995), artifactual components corresponding to pulses, eye blinks or residual scanner artifacts were identified by visual inspection, and removed before backprojection (Grouiller et al., 2011). The EEG was subsequently downsampled to 250 Hz and for each patient IED were visually identified and categorized according to their location and morphology by an experienced electroencephalographer (S.V.).

fMRI data sets were acquired using T_2*-weighted single-shot gradient-echo echo-planar-images (GE-EPI). The parameters of each EEG–fMRI acquisition (number of EEG–fMRI runs, number of scans

Table 1
Clinical details.

Patient	Gender/ age	Focus lateralization	Focus localization	Etiology	Scalp EEG focus	icEEG	Resection	Outcome (12 months)
#1	F, 13 years	Left	Frontal	Tuberous sclerosis	L-frontal; L-fronto-temporal	L-fronto-parietal grid, 2 depth electrodes in L-inf frontal tuber and 1 depth in L-midfrontal tuber	Double tuberectomy (left middle frontal gyrus and left inferior frontal gyrus)	Seizure-free
#2	M, 7 years	Left	Fronto-temporo-parietal	Gliotic scar post abscess	L-fronto-temporo-parietal	L parieto-tempo-occipital grid, 5 strips over L-frontal and L-parietal medial cortex, depth electrodes to bilateral hippocampus/amygdala and anterior cingulated cortex	Lesionectomy	Seizure-free
#3	M, 12 years	Right	Temporo-parieto-occipital	Complex hemispheric malformation	R-temporo-occipital + R-central	–	–	–
#4	F, 8 years	Left	Temporal	Perinatal haemorrhage	L-Temporal	–	–	–
#5	M, 12 years	Left	Temporal	Tuberous sclerosis	L-Temporal; L-Frontal	L-fronto-parieto-temporal grid, 7 strips on L-prefrontal, temporal anterior and temporo-basal cortex	Tuberectomy	Seizure-free
#6	M, 30 years	Left	Frontal	Post-traumatic	Bilateral frontal	–	–	–
#7	M, 16 years	Right	Temporal	Hippocampal sclerosis	R-temporal	–	Anterior temporal lobectomy	Seizure-free
#8	M, 8 years	Left	Parieto-occipital	Dysembryoplastic neuroepithelial tumor	Bilateral parieto-occipital	–	Lesionectomy	Seizure-free
#9	F, 26 years	Left	Parietal	Arterio-venous malformation (operated)	L-centro-parietal	–	–	–
#10	F, 37 years	Left	Frontal	Aspecific white matter lesion	L-frontal	L-frontal grid	Superior frontal cortectomy	>50% seizure reduction
#11	M, 30 years	Left	Temporal	Cryptogenic	L-temporal	–	–	–
#12	M, 22 years	Right	Frontal	Cryptogenic	R>L-frontal	–	–	–
#13	F, 48 years	Left	Temporal	Cryptogenic	L-temporal	–	–	–
#14	F, 25 years	Left	Parietal	Focal cortical dysplasia	L-parieto-temporal	L-parietal grid	Lesionectomy	Seizure-free

Description of patients, including, age and gender, etiology, electrophysiological (scalp EEG and intracranial EEG) details, and surgical resection and outcome after 12 months. F/M: female/male, L/R: left/right.

per run, number of EEG electrodes, repetition time (TR), echo time (TE), voxel resolution, flip angle, number of slices) varied across patients and are shown in Table 2. The EPI images were first realigned (rigid-body registration) to the mean image if the acquisition included a single run, or to the first image of the first run if multiple runs were acquired. The motion-corrected EPI images were then smoothed with a spatial isotropic Gaussian filter of 6 mm full width at half-maximum. Finally, fMRI time series were temporally de-trended with a high pass filter with a cut-off period of 128 s. These steps were performed using SPM8 software (Wellcome Trust Centre for Neuroimaging, University College of London, UK). For the purpose of anatomical localization of the IED-related BOLD signal changes, volumetric 3D T1-weighted images acquired were co-registered to the functional EPI images with the align_epi_anat.py program (Saad et al., 2009) available in the AFNI software (Cox, 1996; NIH/NIMH, Bethesda, USA) and all results were visualized in AFNI. In case of surgical resection, the post-operative 3D T1-weighted images were also co-registered to the functional images.

EEG–fMRI information theoretic analysis

Information-theoretic analysis: entropies and mutual information

To investigate how the BOLD signal encodes information on the IED-related activity shown in the EEG by using an information-theoretic approach, three measures must be considered: the entropy of a random signal X, the conditional entropy of X given another random signal Y, and the MI between the two random signals X and Y (Fuhrmann Alpert et al., 2007; Ostwald and Bagshaw, 2011; Panzeri et al., 2008).

The information shared between two signals is directly related to their degree of uncertainty or randomness (Shannon, 1948). The entropy of X, $H(X)$, is a measure that quantifies the degree of uncertainty of X and it is defined as (Cover and Thomas, 1991)

$$H(X) = -\int_x p(x)\log_b p(x)dx, \quad (1)$$

where $p(x)$ is the probability density function (PDF) of the signal X. For base-two logarithms, the entropy is expressed in unit of bits. Note that $H(X)$ is always larger than 0, and it is equal to 0 if X only has one possible value (i.e., zero entropy is equivalent to no variability, and hence no potential to convey information). In contrast, the more variable a signal is, the higher the entropy and the more information it can contain. $H(X)$ maximizes when all possible values are equiprobable (Shannon, 1948).

In practice, signals are typically more variable than expected due to the presence of observation or quantification noise. Similar to regression or correlation analyses, one can be interested in measuring the amount of information available in X conditioned on the value

Table 2
EEG–fMRI acquisition parameters.

Patient	Center	Number of EEG-electrodes	Number of scans per run	TR/TE (ms)	FA	Number of slices	Matrix size	Voxels size (mm^3)
#1, #8	Geneva	64	1100	1500/35	85°	25	64×64	3.75×3.75×5.5
#2	Geneva	64	1100/500	1500/35	85°	25	64×64	3.75×3.75×5.5
#3	Geneva	64	400	1200/35	90°	20	64×64	3.75×3.75×5.5
#4	Geneva	64	1500	1500/35	85°	25	64×64	3.75×3.75×5.5
#5, #9	Geneva	64	600	1980/30	90°	32	64×64	3×3×3.75
#6	Geneva	64	559	1980/30	90°	32	64×64	3×3×3.75
#7	Geneva	64	1100/188	1500/35	85°	25	64×64	3.75×3.75×5.5
#10, #11, #13, #14	London	32	400/400	3000/30	90°	43	64×64	3×3×3
#12	London	32	400/400/400	3000/30	90°	43	64×64	3×3×3

TE: echo time, TR: repetition time, FA: flip angle.

of another signal of interest Y. The conditional entropy of X given Y, $H(X|Y)$, is defined as (Cover and Thomas, 1991)

$$H(X|Y) = -\int_y \int_x p(x,y)\log_b p(x|y)dxdy = -\int_y p(y)\int_x p(x|y)\log_b p(x|y)dxdy \quad (2)$$

where $p(x|y)$ is the conditional PDF of X conditioned on Y. If knowledge of Y reduces the entropy of X, it indicates that some amount of information is shared by both signals. Consequently, the MI between X and Y, $I(X;Y)$, is given by:

$$I(X;Y) = H(X) - H(X|Y), \quad (3)$$

where $I(X;Y) \geq 0$, and $I(X;Y) = 0$ only if X and Y have no relation. In that situation, the knowledge of Y does not give any indication of the possible value of X and the entropy of X is the same either unconditional or conditional to Y; i.e., when $H(X) = H(X|Y)$. On the contrary, if the value of Y provides all information to infer the value of X, the latter is not uncertain anymore (i.e. $H(X|Y) = 0$), and MI is maximal. Therefore, larger values of $I(X;Y)$ indicate that both signals are closely related. Finally, we also note that the MI is a balanced, symmetric metric, i.e. $I(X;Y) = I(Y;X)$.

Information-theoretic analysis of BOLD signal and IED-related activity

For the computation of the mutual information $I(X;Y)$, we considered that X corresponds to the magnitude of the BOLD fMRI time series at each voxel, and Y is a time series describing the epileptic activity on the EEG data at the fMRI time resolution (EEG–fMRI score). As for X, the fMRI voxel time series were z-normalized to have zero mean and unit variance prior to the computation of the MI. As for Y, we first defined an EEG-score indicating ON ($Y=1$) and OFF ($Y=0$) periods of interictal epileptic activity with a temporal resolution of 250 Hz. The ON periods corresponding to each IED were represented with duration of one TR starting at the onset of the IED. If successive IED events coexisted within one TR, we considered no change in the amplitude of Y (i.e. $Y=1$) as if ON periods overlapped in time. The EEG-score time series at 250 Hz temporal resolution was then down-sampled to the fMRI time resolution (TR) to create the time-series Y used for the computation of the MI. We term this time series as the EEG–fMRI-score because it has the same temporal resolution as the fMRI signal. In case multiple runs of fMRI acquisition were acquired, the z-normalized fMRI voxel time series and the corresponding EEG–fMRI-scores were concatenated in time.

Analogous to the approach used in Fuhrmann Alpert et al. (2007), the MI was computed for each voxel at successive TR latencies by shifting the EEG–fMRI score in time (range between 0 and 12 s). Evaluation of the MI at multiple time latencies is required in order to account for the delay of the haemodynamic response with respect to the onset of the IED event. IED-related EEG data prior to the onset of the fMRI acquisition was taken into account in the computations. In other words, when shifting the EEG–fMRI-scores $Y=1$ observations were marked in the EEG–fMRI score if interictal epileptic activity was observed in the EEG during previous latencies to the onset of the fMRI acquisition, or $Y=0$ otherwise.

MI values were estimated and corrected for bias with the information theory toolbox for Matlab (http://www.ibtb.org; Magri et al., 2009). In brief, the PDF required to compute $H(X)$, $H(X|Y)$ and $I(X;Y)$ with Eqs. (1)–(3) were empirically estimated as histograms with 15 bins uniformly distributed over the entire range of amplitude values of the fMRI voxel time series. Since the PDF are estimated from a limited number of observations, they are subject to statistical error and necessarily fluctuate around the true PDF. These finite-sample fluctuations lead to a possible systematic upward bias in the raw MI values (also often called "plug-in" estimates in the literature) (see Panzeri et al., 2007 for review). Hence, the plug-in MI values were then corrected for bias with the Panzeri and Treves procedure (Panzeri and Treves, 1996) implemented in the toolbox. The choice of a specific number of bins critically influences bias control and sensitivity to information contained in the data (Ince et al., 2012; Ostwald et al., 2010). Our choice for the number of bins was validated as this value corresponded to the minimum number of bins in which the PT-bias corrected MI values achieved a plateau over a large range of bin numbers for all datasets (data not shown).

The above MI analysis yields four-dimensional data sets consisting of the MI values at every voxel and at successive latencies and that reflect the dynamics of the IED-related effects in the fMRI signal. Consequently, three maps were created to summarize the results: 1) a map of the maximum of the MI across latencies in order to localize voxels with high MI statistics regardless of the latency; 2) a map showing the latency at which the value of the MI is maximum. This map was created because different voxels may have equal maximum MI statistics but at different latencies, which illustrates the temporal ordering of the IED-related BOLD activity, and voxels with the earliest latencies can be compared with the location of the expected epileptogenic focus (LeVan et al., 2010b); and 3) a map with the amplitude of the HRF at the latency where the maximum MI occurred because the MI can only take positive values and hence cannot reveal whether IED-related BOLD signal changes were positive (activation) or negative (deactivation), the latter information being important for the interpretation of the results. For that purpose, we estimated the average shape of the HRF in response to the IED with cubic spline functions using the 3dDeconvolve function in AFNI (Cox, 1996; NIH/NIMH, Bethesda, USA).

In order to determine voxels with statistically significant IED-related effect, MI maps were thresholded with a nonparametric statistical procedure. Nineteen subject-specific surrogate datasets were created with an identical spatio-temporal correlation structure to the original fMRI data using a four-dimensional wavelet resampling approach that decorrelates the data in space and time and allows random sign permutations (Patel et al., 2006). Each surrogate dataset was then analyzed with the MI procedure described above. The result of the surrogate analyses was used to sample the probability distribution of the MI statistics under the null hypothesis for each patient individually, where the

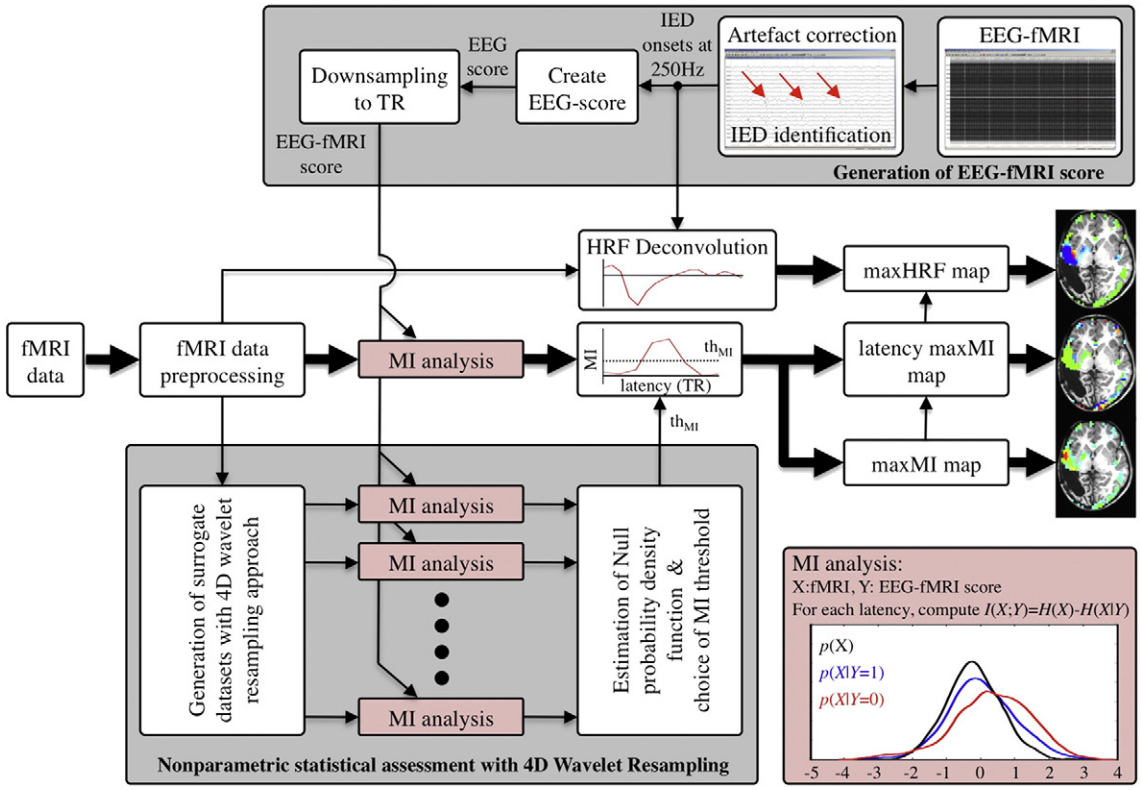

Fig. 1. Schematic diagram of the information theoretic approach. The EEG recorded in the MR scanner is corrected for gradient- and pulse-artifacts. The time of occurrence of IED peaks are marked and the EEG score indicating the existence of epileptic activity is created and finally downsampled to the temporal resolution of fMRI (TR) to generate the EEG–fMRI score (top gray shaded square). The fMRI data is first preprocessed (rigid-body registration for motion correction, spatially smoothed, high pass filtered and z-normalized). The MI between the fMRI voxel time series and the EEG–fMRI score is computed based on the entropy and conditional entropy (bottom right red shaded square) at multiple latencies by shifting the EEG–fMRI score, resulting in an MI time course. The shape of the HRF is deconvolved based on the IED timing. Significant MI statistics are those exceeding a thresholded th_{MI}, which is chosen according to nonparametric statistical procedure where 19 surrogate datasets created with a 4D wavelet resampling approach are analyzed in the same way as the original dataset and the PDF of the MI statistics under the null is estimated (bottom gray shaded square). To summarize the results, three maps are generated: a maximum MI map, a latency map showing the latency at which the maximum MI occurs, and a map plotting the amplitude of the HRF at the latency of the maximum MI. (For interpretation of the references to color in this figure legend, the reader is referred to the web version of this article.)

number of samples is equal to the number of surrogates multiplied by the number of voxels and number of latencies. For each patient, two different thresholds were considered with decreasing statistical significance. First, an initial MI threshold was set according to the maximum value of MI across all surrogate datasets, latencies and voxels. This value corresponds to a nonparametric $p<0.05$ corrected across voxels and latencies (labeled as NP-C) (Nichols and Holmes, 2002). If setting this threshold yielded MI maps with reduced statistical power or the maximum MI statistic was not located in a cluster within the target area (see below), we also considered an additional threshold chosen as the value of MI for which the cumulative distribution function of the MI statistic under the null hypothesis corresponded to $p<0.001$ uncorrected across voxels and latencies (NP-UNC). For both thresholds, a minimum cluster size of 5 voxels was applied to avoid detecting IED-related BOLD activations in isolated voxels.

A schematic diagram describing the steps of the information theoretic approach is shown in Fig. 1.

EEG–fMRI general linear model analysis

The fMRI data was also analyzed by means of two GLM-based approaches as implemented in SPM8 (FIL/UCL). These GLM approaches are constrained by initial assumptions (linearity of the neurovascular coupling of the BOLD response, gaussianity of the model residuals, as well as a specific HRF model for the GLM1 approach) that will be tested by the more flexible MI approach.

GLM1

Three IED-related regressors resulting from the convolution of delta functions (zero-duration events) at the time of the IED with the canonical HRF and its temporal derivative and partial derivative with respect to the dispersion parameter, i.e. the Informed Basis Set (IBS) model (Friston et al., 1998).

GLM2

Finite Impulse Response (FIR) model (Buckner et al., 1996; Dale and Buckner, 1997); i.e., IED-related regressors were created as consecutive box-car functions of duration TR seconds starting at the IED onsets and spanning for a duration of the haemodynamic response of 24 s. Similar to the information-theoretic approach, the FIR analysis can identify voxels that show IED-related BOLD signal changes with a consistent shape but without imposing an explicit haemodynamic model such as the canonical HRF adopted in the IBS model.

Furthermore, the time series of the 6 translation and rotation parameters estimated during motion-correction were also modeled as effects of no interest in both GLM analyses in order to capture motion-related effects. Both models were fitted via a Restricted Maximum Likelihood estimator considering a first-order autoregressive process (AR) plus white noise to model the serial correlations of the residuals. Therefore, both approaches assume a linear model for the BOLD response.

The statistical parametric map (SPM) of the IBS model (GLM1) was set on the F-statistic of the three IED-related regressors (i.e., the canonical HRF plus the temporal and dispersion derivatives). An SPM with the

t-statistic for the weight of the IED-related canonical HRF regressor was also calculated for GLM1 to establish the sign of the BOLD changes. Regarding the FIR model (GLM2), the SPM was created by performing an F-test comprising all basis-set regressors. In both cases, two significance levels were considered: $p<0.05$, family-wise error (FWE) corrected for multiple comparisons across the whole brain, and a further inspection of the maps at $p<0.001$ uncorrected. Similarly to the MI maps, a minimum cluster size of 5 voxels was also considered at both thresholds.

Assessment of concordance

In those patients who showed seizure freedom or >50% reduction in seizure frequency after surgical resection, a target area was defined as the resection area and its direct proximity (<15 mm from resection margins and within the same sublobar cortical region) (Grouiller et al., 2011). The distance was introduced to account for discrepancies in the spatial concordance between BOLD signal changes and neuro-electrical activity (Bénar et al., 2006; Disbrow et al., 2000). For those cases where neither icEEG nor surgical resection was available we defined a target lobe based on the focus of non-invasive scalp EEG recordings and structural imaging (Grouiller et al., 2011; Vulliemoz et al., 2010b). For all analyses, the degree of concordance was categorized into three groups: High Concordance (++) when any cluster with $p<0.05$ corrected (either NP-C for the MI analysis or FWE for the IBS and FIR analyses) or the cluster with the statistical maximum with $p<0.001$ (NP-UNC or UNC) is located within the target area or lobe; Low Concordance (+) when any cluster with $p<0.001$ (NP-UNC or UNC) was located within the target area or lobe; and Discordance (D) when the ensuing maps showed absence of IED-related BOLD cluster in a target area or lobe at uncorrected statistical significance, or diffuse bilateral BOLD changes that prevented the delineation of a candidate epileptogenic cluster in the target area. In those cases where a concordant cluster was found, we also evaluated whether the latency of the maximum MI coincides with the latency of the maximum signal change of the HRF, and the polarity of the HRF at both latencies.

Results

Concordance

The results of the MI, GLM1 (IBS) and GLM2 (FIR) analyses are summarized in Table 3. The results of illustrative case reports are shown in Figs. 2–5 and the maps for the other subjects are given as supplementary material.

Among the 14 patients, the MI analysis found IED-related BOLD signal changes that were spatially concordant with the target area in 8 patients (7/1 with high/low concordance). GLM1 and GLM2 yielded concordant results in 8 (8/0) and 7 (7/0) patients, respectively. The 7 cases where MI analysis was highly concordant (++) with electro-clinical localization or surgical resection were also labeled as highly concordant with the IBS and FIR analyses, and these studies had a large number of IED (range 133–1407) except for patient #10. Moreover, all analyses yielded discordant results in 5 cases (patients #4, #5, #7, #8 and #9). We also observed discordant maps for patients #3 with the MI and FIR analyses, and for patient #14 with the IBS and FIR models. Further assessment indicated that discordance might be the result of motion-related artifacts in the fMRI signal in two cases (patients #4 and #7), and widespread IED-related BOLD signal changes that impede the localization of the epileptic foci in two cases (patients #5 and #8). The cluster closest to the target area exhibited the highest statistical value in 5/8 patients for MI (maximum MI), 3/8 for IBS (F-value), and 4/7 for FIR (F-value). In all cases, the polarity of the IED-related BOLD signal change at the latency with the maximum MI matched the polarity fitted with the IBS model. The concordant MI clusters showed positive IED-related BOLD signal changes in 4/8 and negative changes in 4/8.

Table 3
Results.

Patients	IED during each fMRI run	IED-interval (mean/STD)	Number of ON time points	Mutual information		Informed basis set			Finite impulse response		
				Degree of concordance	Maximum in target area ?/polarity of concordant cluster/latency of maxMI in concordant cluster/ latency maxMI = latency MaxHRF? (If no, same polarity)	Columns in design matrix	Degree of concordance	Maximum in target area?/ polarity of concordant cluster	Columns in design matrix	Degree of concordance	Maximum in target area?
#1	81	14.86/22.43	74	++	Yes/pos/3–4.5 s/yes	10	++	No/pos	23	++	No
#2	945/462	1.65/8.41	937	++	Yes/neg/4.5–6 s/yes	20	++	Yes/neg	25	++	Yes
#3	30	9.44/14.79	24	D	n.a.	10	++	No/neg	27	D	n.a.
#4	29	74.76/95.93	26	D	n.a	10	D	n.a	23	D	n.a.
#5	327	3.45/6.37	202	D	n.a.	13	D	n.a.	31	D	n.a.
#6	109	7.62/24.80	66	++	Yes/neg/6–8 s/no (yes)	10	++	Yes/neg	19	++	Yes
#7	5/25	63.27/113.56	30	D	n.a.	20	D	n.a.	25	D	n.a.
#8	257	5.94/15.16	127	D	n.a.	10	D	n.a.	23	D	n.a.
#9	12	46.54/86.35	12	D	n.a.	10	D	n.a.	19	D	n.a.
#10	25/15	36.24/97.72	12	++	No[a]/pos/3 s/yes	20	++	No[a]/pos	30	++	Yes
#11	122/101	10.62/16.88	151	++	Yes/neg/3 s/yes	20	++	No[a]/neg	30	++	No[a]
#12	180/114/69	9.78/15.69	216	++	Yes/pos/3 s/yes	30	++	Yes/pos	45	++	Yes
#13	87/117	10.37/15.54	151	++	No[a]/neg/3 s/yes	20	++	No[a]/neg	30	++	No[a]
#14	183/53	10.11/6.76	209	+	No/pos/6 s/yes	20	D	n.a.	30	D	n.a.

Number of IED detected in scalp EEG in each run, time interval between successive IED (average and standard deviation), number of ON time points in EEG–fMRI score considering all runs, MI results and results of SPM analysis with the Informed Basis Set (i.e. canonical HRF and its temporal and dispersion derivatives) and the Finite Impulse Response models. Degree of concordance: ++: high concordance, +: low concordance, D: discordant). n.a.: not applicable.

[a] Global statistical maximum occurred in areas related to the Default Mode Network (DMN).

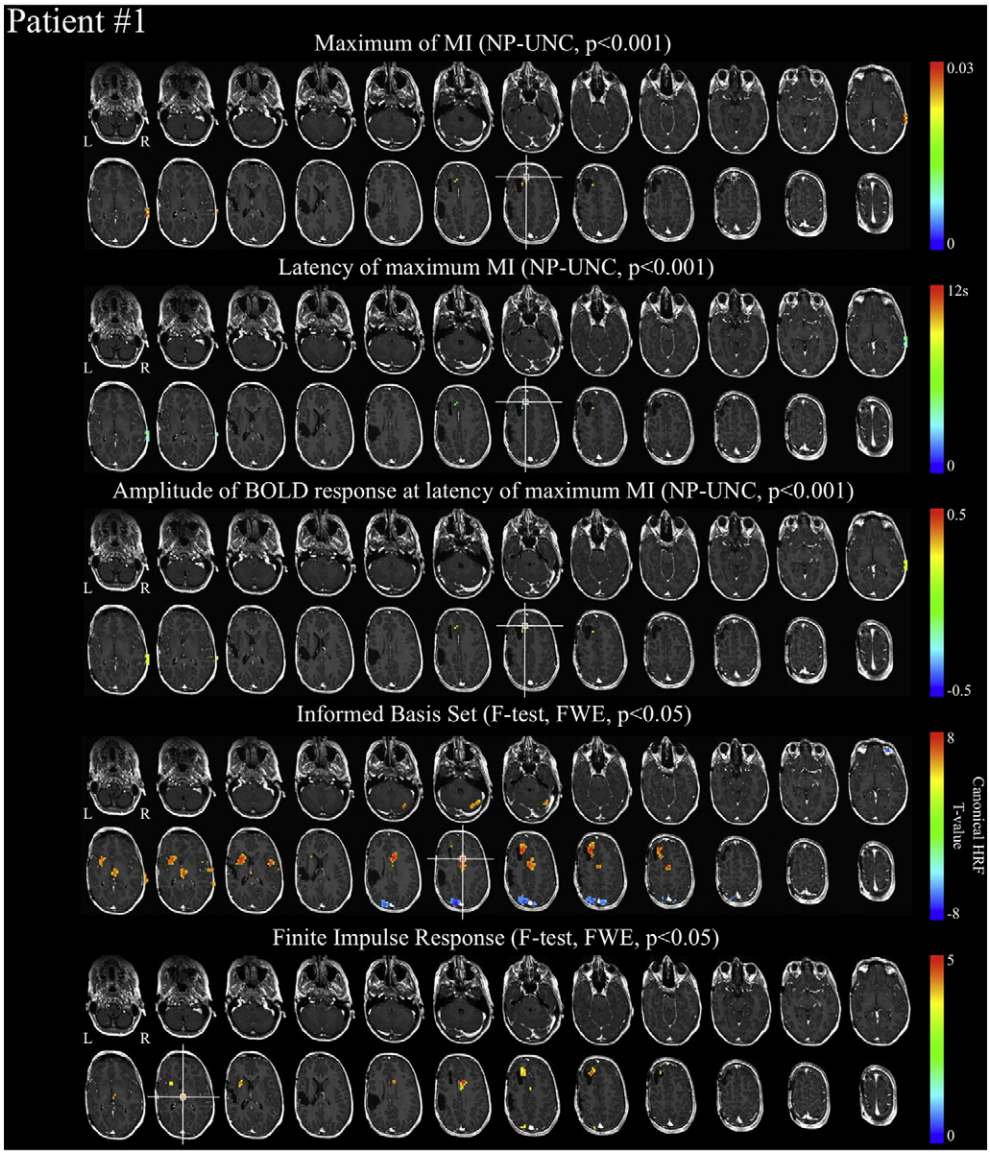

Fig. 2. Patient #1: tuberous sclerosis with 2 tubers in left anterior frontal and left inferior frontal. Scalp EEG focus in left frontal and left fronto-temporal, confirmed by intracranial EEG. Seizure-free after resection of both tubers. fMRI maps: (a) maximum MI, b) latency of maximum MI, c) amplitude of the HRF at latency of maximum MI, thresholded at non-parametric uncorrected (NP-UNC) $p<0.001$: cluster with maximum MI close to tuber in left anterior frontal; d) IBS model: SPM depicts the t-statistic of the canonical HRF regressor, where the threshold is set based on the F-statistic of the canonical HRF, temporal and dispersion derivative regressors with FWE-corrected $p<0.05$: clusters localized close to both tubers in left anterior frontal and left inferior frontal; e) FIR model: SPM depicts the F-statistic of the FIR regressors with FWE-corrected $p<0.05$: concordant clusters in both tubers, the cluster in left inferior frontal can be seen at uncorrected $p<0.001$. Maps have a minimum cluster size of 5 voxels and are overlaid on postoperative T1-weighted image in individual space. Voxels with the global statistic maximum are marked with a cross.

In general, the latency maps demonstrated large variability across subjects and cortical regions with regard to the time when the maximum MI between the EEG-score and the fMRI signal occurs. In patients #10, #12 and #14 the maximum MI of the concordant clusters occurred at short latency (0–3 s) and this also coincided with the maximum signal change of the estimated BOLD response. This observation contrasts with the expected time-to-peak of 5–6 s after the neuronal event of the canonical HRF. Hence, to examine whether a peak at zero or one latency reflects the effect of the preceding IED instead of the current one, we calculated the average and standard deviation of the time interval between successive IED (see Table 3). We observed no systematic differences in the MI results that could be explained in terms of the interval between IEDs. The latency of the maximum MI in the concordant negative BOLD cluster of patient #6 occurred earlier than the latency of maximum BOLD signal change.

In the following, the description of the individual results is grouped with respect to the degree of concordance (i.e. concordant and non-concordant cases) and the reliability of the findings in terms of the availability or not of invasive clinical assessment.

Cases with concordant MI results and invasive clinical assessment (icEEG and surgical resection)

Patient #1

The results of the MI, IBS and FIR analyses are shown in Fig. 2. This patient had tuberous sclerosis with two epileptogenic tubers in left anterior frontal and left inferior frontal regions. The EEG focus was

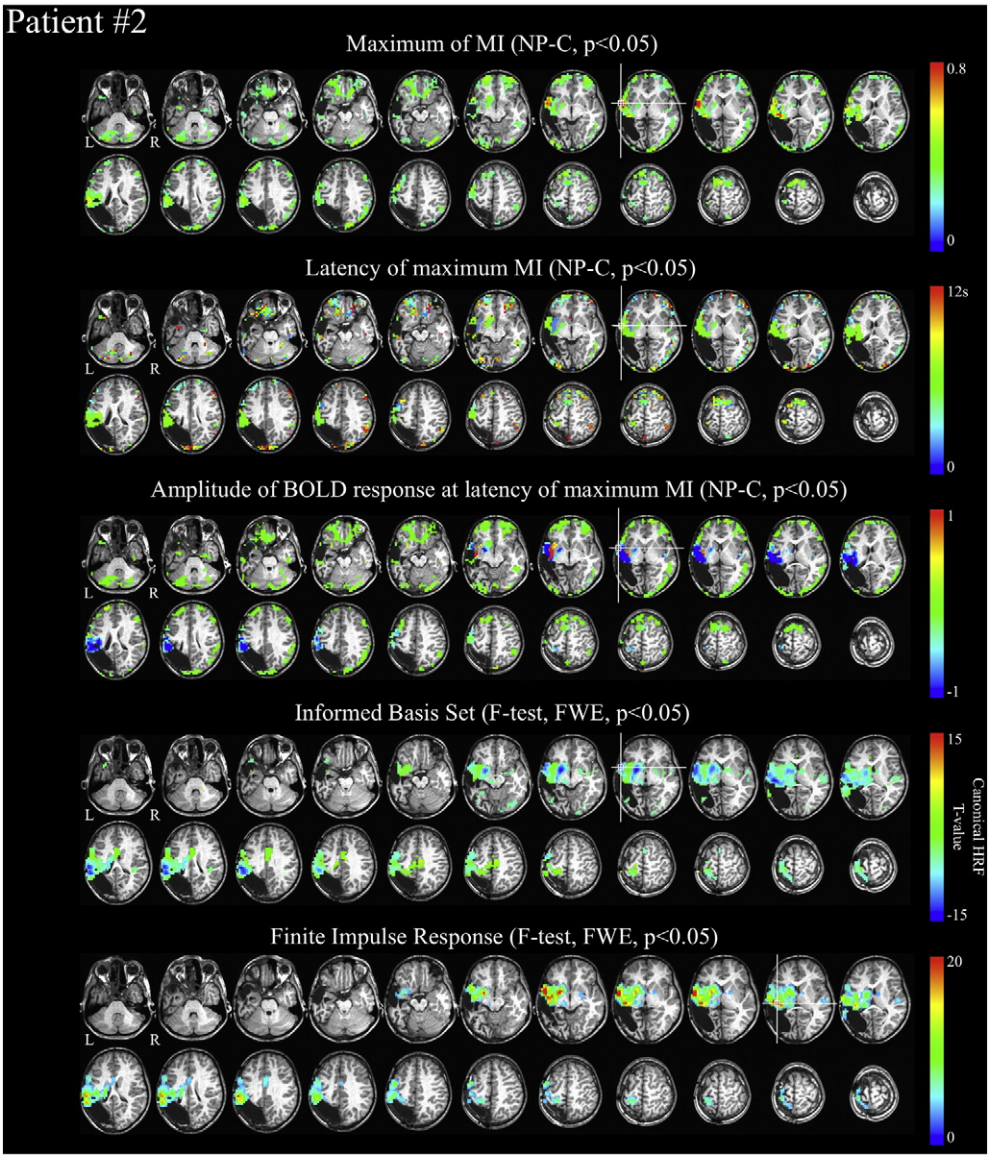

Fig. 3. Patient #2: left hemispheric epilepsy symptomatic of a large abscess gliotic scar. EEG focus in left fronto-temporo-parietal, confirmed by icEEG. Seizure-free after lesionectomy. Maps in figure: (a) maximum MI, b) latency of maximum MI, c) amplitude of the HRF at latency of maximum MI, thresholded at non-parametric corrected (NP-C) $p<0.05$; d) IBS model: SPM depicts the t-statistic of the canonical HRF regressor, where the threshold is set based on the F-statistic of the canonical HRF, temporal and dispersion derivative regressors with FWE-corrected $p<0.05$; e) FIR model: SPM depicts the F-statistic of the FIR regressors with FWE-corrected $p<0.05$. All maps depict concordant clusters with significant IED-related BOLD signal changes in left perisylvian regions (superior temporal, lateral inferior frontal), sensorimotor (precentral and postcentral gyri) and lateral parietal cortex. The latency MI map indicates early MI-significant positive IED-related signal changes in left anterior insula, in contrast to the negative IED-related signal changes observed in the rest of the areas. Maps have a minimum cluster size of 5 voxels and are overlaid on postoperative T1-weighted image in individual space. Voxels with global statistic maximum are marked with a cross.

localized in left frontal and fronto-temporal areas. Intracranial EEG recording showed independent involvement of both tubers in the generation of seizures and the patient was seizure free after surgical resection of both tubers. The maximum MI values (shown with cross) were obtained in a cluster located close to the tuber in left anterior frontal and thus we categorized the MI results as highly concordant. Clusters concordant with both tubers were found by the IBS and FIR analyses (anterior frontal at $p<0.05$ FWE, and inferior frontal at $p<0.001$ UNC) (maps not shown in this figure).

Patient #2

Fig. 3 depicts the MI, IBS and FIR maps for this patient with left hemispheric epilepsy symptomatic of a large abscess gliotic scar. The EEG focus was localized in left fronto-temporo-parietal areas, confirmed by icEEG. The patient was seizure-free after surgical resection of these areas. The three methods showed a large degree of correspondence of significant IED-related BOLD signal changes in perisylvian regions, sensorimotor (postcentral and precentral gyri) and lateral parietal areas in the left hemisphere ($p<0.05$ NP-C, and FWE). The MI latency map shows that the maximum MI in the left insula occurred earlier (latency of 1 TR) than in clusters with larger MI values (left inferior frontal, left frontal operculum, left superior temporal gyrus, left posterior planum temporale and left basal ganglia). The MI values in the left insula return to achieve high statistical significance at later latencies and corresponding to negative BOLD changes, illustrating that MI values at this area exhibited a bimodal temporal pattern with two peaks achieving high statistical significance at separated latencies. Voxels in this area exhibit low T-values at the IBS map.

Patient #10

Fig. 4 shows the MI, IBS and FIR maps for this patient where the EEG–fMRI-score only included 12 ON time points at the fMRI resolution with

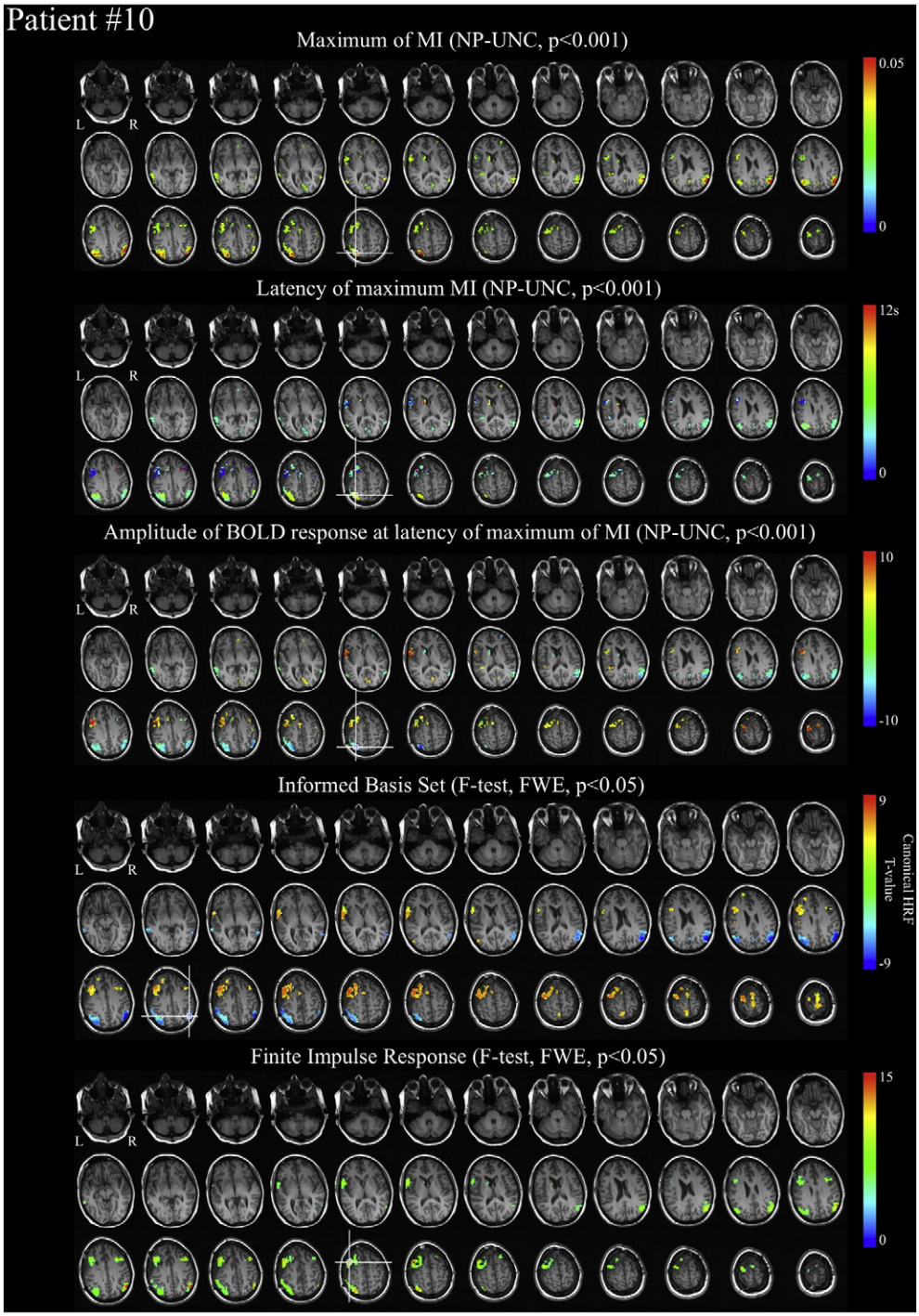

Fig. 4. Patient #10: left frontal (non-lesional) epilepsy. EEG focus in left frontal. 50% reduction in seizure frequency after superior frontal cortectomy. Maps in figure: (a) maximum MI, b) latency of maximum MI, c) amplitude of the HRF at latency of maximum MI. Concordant clusters in target area (left superior frontal) were found at non-parametric corrected (NP-C) $p<0.05$, but maps are shown at non-parametric uncorrected (NP-UNC) $p<0.001$ for better visualization; d) IBS model: SPM depicts the *t*-statistic of the canonical HRF regressor, where the threshold is set based on the F-statistic of the canonical HRF, temporal and dispersion derivative regressors with FWE-corrected $p<0.05$; e) FIR model: SPM depicts the F-statistic of the FIR regressors with FWE-corrected $p<0.05$. All maps depict concordant clusters of positive IED-related BOLD signal changes in left frontal regions and negative ones in parietal areas of the default mode network. Maps have a minimum cluster size of 5 voxels and are overlaid on postoperative T1-weighted image in individual space. Voxel with global statistic maximum are marked with a cross.

possible IED-related BOLD activity from the 40 IED detected on the scalp EEG. This patient had a non-specific white matter lesion. The EEG focus was localized in left frontal areas, confirmed by icEEG. The patient experienced more than 50% reduction of epileptic seizures after partial resection of the left superior frontal gyrus, which was defined as the target area. The MI results revealed clusters in frontal regions with positive BOLD changes, whereas clusters with the negative BOLD changes were observed in lateral parietal cortices and precuneus. The MI latencies displayed that IED-related BOLD changes were initially observed in left inferior frontal areas, which later propagated into left middle frontal areas (exceeding the corrected threshold $p<0.05$ NP-C), left superior frontal and right middle frontal areas, and ventrally into the lateral parietal areas of both hemispheres (exceeding $p<0.05$ NP-C) and precuneus, suggesting the involvement of regions typically associated

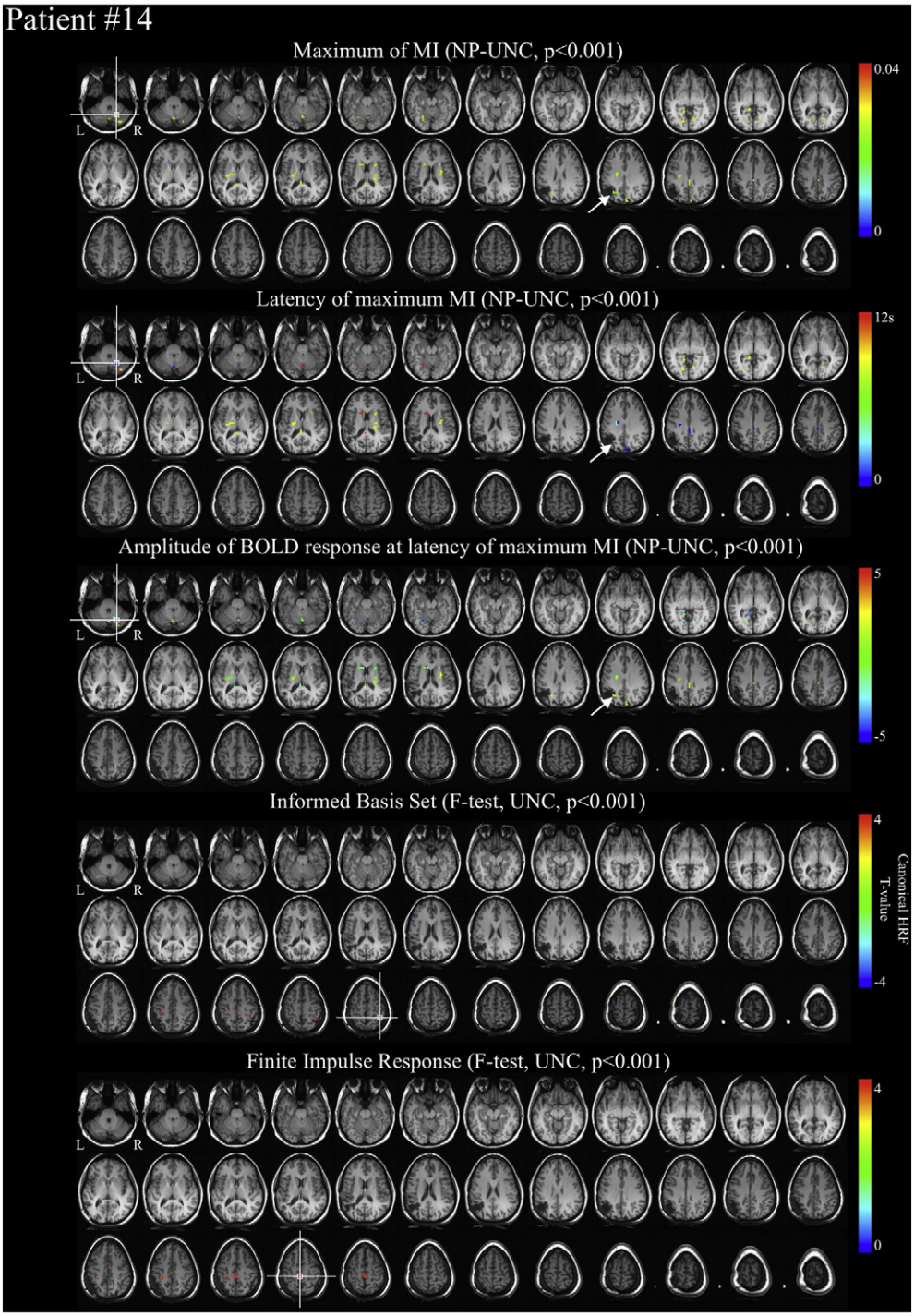

Fig. 5. Patient #14: focal cortical dysplasia (FCD). EEG focus in left parieto-temporal, confirmed by icEEG. Seizure-free after lesionectomy. Maps in figure: (a) maximum MI, b) latency of maximum MI, c) amplitude of the HRF at latency of maximum MI, thresholded at non-parametric uncorrected (NP-UNC) $p<0.001$: low significant concordant clusters in the target area of left posterior parietal temporal region, as confirmed with icEEG and surgical resection (shown with arrows); d) IBS model: SPM depicts the *t*-statistic of the canonical HRF regressor, where the threshold is set based on the F-statistic of the canonical HRF, temporal and dispersion derivative regressors with uncorrected (UNC) $p<0.001$; e) FIR model: SPM depicts the F-statistic of the FIR regressors with UNC $p<0.001$. No clusters are found in the target area with either IBS or FIR models. Maps have a minimum cluster size of 5 voxels and are overlaid on postoperative T1-weighted image in individual space. Voxels with global statistic maximum are marked with a cross.

with the default mode network (Kobayashi et al., 2006; Laufs et al., 2007; Raichle et al., 2001). The MI analysis also showed good concordance with the IBS and FIR analyses.

Patient #14

Fig. 5 shows the results for this patient with focal cortical dysplasia in left parieto-temporal areas. Scalp EEG and icEEG delineated a seizure onset zone in this region and the patient was seizure free after surgical resection of this area. The MI results were categorized as low concordant ($p<0.001$ NP-UNC) revealing a widespread pattern of cortical and subcortical IED-related BOLD signal changes, including two clusters of positive BOLD signal within the target area (shown with arrows). Both IBS and FIR analysis showed discordant results with no clusters in the target area, although by lowering the statistical threshold below $p<0.001$ UNC we observed clusters extending into areas anterior to the resected region.

Cases with concordant MI results and non-invasive clinical assessment

High concordant results were also obtained with MI analysis in patients #6, #11, #12 and #13 where the target area was defined at the lobular level based on scalp EEG focus since no icEEG or surgical resection was performed (maps shown in Supplementary figures).

Patient #6 had extensive traumatic lesions affecting the left hemispheres and the right frontal lobe, as well as bilateral frontal EEG abnormalities. The clusters with negative BOLD signal changes were observed in target anterior medial and lateral frontal areas, predominantly in the right hemisphere. The IBS and FIR maps were in close agreement with the MI results, but the latter showed less number of voxels with significant MI values ($p<0.05$ NP-C). In patient #11 with cryptogenic epilepsy, the EEG focus was localized in left temporal areas. The three methods were categorized as highly concordant identifying negative left superior temporal IED-related BOLD signal changes in agreement with electro-clinical findings, although the MI maps showed considerably less clusters than the IBS and FIR maps (MI maps in Supplementary figure are shown at $p<0.001$ NP-UNC for the sake of visualization, but concordant clusters achieved corrected statistical significance $p<0.05$ NP-C). In both patients #6 and #11, negative IED-related BOLD signal clusters were observed in posterior parts of the DMN (precuneus and lateral parietal areas).

In patient #12, who had cryptogenic epilepsy, the EEG focus was localized in frontal areas with predominance of the right hemisphere. The MI analysis revealed positive IED-related BOLD changes in the middle and superior frontal areas in both hemispheres with higher MI values in right frontal, in agreement with the EEG. Both FIR and IBS analyses showed IED-related BOLD signal clusters in bilateral inferior frontal and insula. The FIR maps revealed additional clusters in posterior regions of the DMN such as posterior cingulate gyrus, precuneus, lateral temporo-parietal, and the occipital lobe.

In patient #13, who had cryptogenic epilepsy, the EEG focus was localized in left temporal regions. The MI analysis obtained concordant results revealing negative IED-related BOLD clusters in the left middle temporal gyrus and the left insula ($p<0.001$ NP-UNC), whereas positive clusters were observed in hippocampal (medial temporal) regions in both hemispheres ($p<0.05$ NP-C) (MI maps in Supplementary figure are shown at $p<0.001$ NP-UNC for better visualization). Both FIR and IBS maps showed large correspondence with the MI maps at corrected statistical significance ($p<0.05$ FWE). The maximum statistics for all methods were seen in clusters located in DMN areas (left angular gyrus, posterior cingulate, and precuneus) associated with negative BOLD changes. The latency MI map suggests fast IED-related BOLD changes (MI is maximum at zero latency) in hippocampal regions of both hemispheres, left angular gyrus and posterior cingulate, and then propagation to left lateral temporal areas, left angular gyrus, left insula, precuneus, and left anterior frontal areas. The IBS analysis also revealed clusters of negative IED-related BOLD changes in the right angular gyrus and positive ones in primary visual and premotor areas of both hemispheres.

Cases with discordant MI results

Five discordant cases for the MI analysis (patients #4, #5, #7, #8 and #9) were also categorized as discordant for the IBS and FIR analyses. In contrast, the results for patient #3 were categorized as discordant for MI and FIR, but highly concordant with the IBS model although invasive validation is lacking in this case.

In two of these cases (patients #4 and #7), no IED-related BOLD signal changes were found with MI contrary to the multiple discordant clusters found with the IBS and FIR analyses. These 2 cases showed important motion artifacts: in patient #4 large head jerks (>0.2 mm/scan) occurred during scanning, corresponding to 45.2% of the scans being affected by motion-related effects, when considering the motion-related effects due to each head jerk that span 4 scan repetition times due to spin-history effects (Lemieux et al., 2007). In patient #7, only 4.2% of the scans coincided with head jerks, but a significant head movement (>5 mm/scan) in the middle of the run caused a prolonged BOLD signal change interfering with the MI analysis.

In patient #9, who suffered from an arterio-venous malformation, the EEG focus was localized in left centro-parietal regions. Sequelae of arterio-venous malformation bleeding causing a drop in the BOLD signal might have affected the detection of concordant clusters with the three methods. In addition, a low number of IED were identified on the scalp EEG (12 IED, left centro-parietal) during the EEG–fMRI acquisition.

Patient #3 suffered from a complex malformation in the right hemisphere. No validation by icEEG and/or postoperative seizure reduction is available for this patient. MI analysis revealed no voxels exceeding the uncorrected threshold ($p<0.001$ NP-UNC). In contrast, the IBS map ($p<0.05$ FWE) showed a negative IED-related BOLD cluster in the right occipital cortex concordant with our definition of the target area based on the scalp EEG focus. However, the highest T-statistics of the IBS model and all clusters shown in the FIR map ($p<0.001$ UNC) were located within the cyst of cerebro-spinal fluid where no cortical tissue exists.

Patient #5 suffered from tuberous sclerosis and showed multifocal IED. Intracranial EEG showed that the most irritative tuber concordant with the seizure onset zone was in the left temporal lobe, although less rhythmic spikes were observed in frontal areas in both hemispheres. Similarly to the icEEG, the scalp EEG showed a complex pattern of IED originating from bilateral frontal, left temporal, left centro-temporal and left fronto-temporal. Here, we report the results of the analysis with the left fronto-temporal and bilateral frontal IED that were considered as the most clinically relevant. The patient was seizure free after resection of the left anterior temporal lobe, which we defined as the target area for concordance evaluation. Concordant positive clusters were observed in the resected areas with the three methods at the uncorrected threshold ($p<0.001$ NP-UNC; and UNC). Nevertheless, the maps mainly displayed positive IED-related BOLD signal changes involving frontal areas in both hemispheres and right lateral parietal areas, along with negative ones in the precuneus, mainly reflecting the propagation of epileptic activity and thus were categorized as discordant for the three analyses.

Patient #8 had a dysembryoplastic neuroepithelial tumor and the scalp EEG focus indicated IED originating in bilateral parieto-occipital areas. All fMRI analyses showed widespread bilateral IED-related BOLD changes at the highest statistical threshold ($p<0.05$ NP-C and FWE). The IBS and FIR maps were more diffuse than the MI maps, showing significant IED-related BOLD signal changes across most of the neocortex.

Discussion

Our information-theoretic approach to map BOLD signal changes related to focal interictal epileptic activity was able to localize the irritative zone in 8/14 cases, as confirmed by invasive electrophysiology or post-operative follow-up in 4/8 of the concordant patients. Our results in this group of patients with a wide range of epileptic etiologies, varying numbers of IED, and localization of epileptogenic areas, validate to a certain extent the assumptions typically accepted in EEG-correlated fMRI analysis for spatial localization of focal epilepsy with regard to (1) the shape of the haemodynamic response, which can be described based on the informed basis set (i.e., the canonical HRF) (2) the linearity of the signal model and (3) the use of T- and F-statistics, which rely on the gaussianity of the model residuals. Not only did we observe large correspondence between the MI maps and the GLM-based IBS and FIR maps in the concordant cases (patients #1, #2, #6, #10, #11, #12 and #13), but also we found that the discordant GLM-based results could not be explained by these limiting assumptions, particularly those with a large number

of interictal events as in patients #5 and #8. The MI latency analysis of data from patients #2 and #13 provided us with useful information about the propagation of IED-related haemodynamic changes. The MI analysis showed improved concordance than the GLM-based methods in one patient (patient #14) in whom the latter exhibited lack of power in detecting IED-related BOLD signal changes. In two other cases (patients #1 and #11), only MI showed a concordant statistical global maximum. In four cases discordant for the 3 methods (patients #4, #7, #8, #9), MI was less sensitive at detecting discordant clusters. These results confirm that an information-theoretic analysis based on the MI between the fMRI signal and the EEG-score can serve as a supplementary tool for more comprehensive analysis techniques used in epileptic studies with concurrent EEG–fMRI.

Neurovascular coupling

The three methods agreed on the degree of concordance in 12 cases (7 highly concordant and 5 discordant). The GLM-based approaches incorporate the linear time-invariant system assumption that haemodynamic responses to IED can be described as a linear convolution of a train of Dirac impulses (events) at the onset of the IED with a temporal basis set, either the canonical HRF plus its temporal and dispersion derivatives, or successive boxcar functions in the FIR model. Alternatively, bursts of consecutive IED could be represented as continuous boxcar functions of epileptic activity with the actual IED duration to improve the statistical results (Bagshaw et al., 2005). Departures from linearity in the BOLD signal have been noted in event-related paradigms with brief and consecutive stimuli where BOLD responses overlap (de Zwart et al., 2009; Heckman et al., 2007; Liu et al., 2010), mimicking the scenario found in cases with very frequent IED detected in the scalp EEG (see Bagshaw et al., 2005; Jacobs et al., 2008; Mirsattari et al., 2006; Vanzetta et al., 2010; Voges et al., 2012, as detailed studies addressing nonlinear effects in the BOLD signal in epilepsy). The large resemblance between the MI, IBS and FIR maps in 4 patients with a wide range of IED frequency (cases #2, #11, #12, and #13) corroborates that, at least in these concordant cases, modeling nonlinear effects is not necessary in order to find concordant clusters in the epileptogenic areas (Vanzetta et al., 2010). In addition, by comparing the IBS maps with those of MI and FIR analyses, one can confirm that the adoption of the canonical HRF plus its temporal and dispersion derivative is a reasonable and practical model for the haemodynamic response in refractory focal epilepsy (Lemieux et al., 2008; Salek-Haddadi et al., 2006; Vulliemoz et al., 2010b). However, we observed that the global statistical maximum was not located in the target area in 3/8 concordant cases for MI (patients #10, #13 and #14), 5/8 cases for IBS (patients #1, #3, #10, #11 and #13) and 3/7 cases for FIR (patients #1, #11 and #13). The global statistical maximum was found in areas belonging to the DMN in patient #13 with the three methods, in patient #10 with the MI and IBS analyses, and in patient #11 with the IBS and FIR methods. These findings are concordant with the large modulation of the BOLD signal in the DMN observed in relation to epileptic activity in the temporal lobe as well as primary and secondary generalized spike and wave discharges, the latter being frequently observed in frontal lobe epilepsy (Gotman et al., 2005; Kobayashi et al., 2006; Laufs et al., 2007; Salek-Haddadi et al., 2006; Vulliemoz et al., 2010b). As mentioned above, the MI analysis of patients #1 and #11 yielded its global maximum in clusters within the target area, but not with the GLM-based methods.

The sign of the BOLD changes in the concordant cluster was always congruent between the BOLD change at the time with maximum MI and the fit of the canonical model, and half of the concordant cases showed negative BOLD changes (4 cases). BOLD signal decreases in brain voxels close and remote to the epileptic onset zone, although frequently observed, are difficult to interpret as multiple factors such as age, sedation, vigilance, spike frequency and type of epilepsy could affect the underlying neuronal, vascular and metabolic mechanisms that originate them (Bagshaw et al., 2004; Jacobs et al., 2008; Kobayashi et al., 2006; Salek-Haddadi et al., 2006). Similar to the GLM-based maps, the MI maps in five patients (three with cryptogenic epilepsy) also revealed negative BOLD signal changes in posterior regions of the "default mode network" (DMN), such as posterior cingulate, precuneus and lateral temporoparietal cortices (Raichle et al., 2001). This has been interpreted as a suspension of the resting neuroelectrical activity and linked with impaired consciousness in generalized seizures as well as temporal lobe epilepsy (e.g. see maps of patient #11) (Gotman et al., 2005; Kobayashi et al., 2006; Laufs et al., 2007; Vulliemoz et al., 2009, 2010b, 2011).

Dynamics of epileptic networks and early BOLD changes

Although the propagation of epileptic activity across the brain take place over timescales of tens or hundreds of milliseconds, BOLD fMRI can help to map the dynamics of the networks associated with interictal (Vulliemoz et al., 2009) and ictal (Donaire et al., 2009; LeVan et al., 2010b; Tyvaert et al., 2009) epileptic activity. Similar to the brain activation sequences obtained from the FIR analysis (Windischberger et al., 2008), we attempted to map the propagation of interictal epileptic activity in the brain by estimating the MI value at successive shifts of the EEG–fMRI score with respect to the fMRI signal (Fuhrmann Alpert et al., 2007). In general, we observed that the MI "time course" had a unique mode and we plotted this preferred latency; i.e., the shift at which MI was maximal, in the latency MI map. However, one must be aware that summarizing sequential information into a single map prevents us from knowing those cases where the MI exhibits a multimodal time course or exceeds the statistical threshold for several lags above, underlying the importance of exploring multiple MI lags (Aghakhani et al., 2004; Bagshaw et al., 2004). For instance, an interesting example of bimodal MI values was found in patient #2, where the anterior part of the left insula in this patient had its maximum MI value at zero lag and later returned to be significant after it was maximal in those areas where the largest MI, T- or F-values were observed. Interestingly, further investigation revealed that the polarity of the BOLD response at the first (and maximum) MI mode was positive, whereas it was negative for the second mode at latencies 4.5–6 s. Hence, this provides an explanation about why this area is mapped with low and negative T-values in the IBS map as the model fits the negative BOLD signal change with similar time-to-peak to the canonical HRF.

The latency MI maps of some patients displayed clusters either close to or distant from the target area at which the maximum MI occurred at lags zero or one TR. The fact that the maximum MI between the fMRI and EEG data occurred at short latencies indicates that the fMRI signal maximally encodes the epileptic activity shown in the scalp EEG, and vice versa, during the first period of the IED-related BOLD response. This result might represent the effect of the preceding IED in case of very frequent spikes but we found no clear relationship between IED rate (measured as the average time interval between IED) and maximum MI occurring at short latencies. Alternatively, this finding supports, without any HRF model, studies suggesting that BOLD signal changes might start prior to the IED seen on the scalp EEG (Hawco et al., 2007; Jacobs et al., 2009; Pittau et al., 2011; Rathakrishnan et al., 2010; Schwartz et al., 2011).

Clinical significance

Most patients had non-lesional imaging or multifocal epileptic activity. In these difficult pharmaco-resistant cases, multimodal information is critical for the clinicians to gain confidence in the localization findings and the additional information gained by MI analysis in two-thirds of the cases can be very helpful. Although methodological advances are still needed to gain clinically relevance from the discordant cases, the most important message of our study is certainly the congruence

between our flexible model and the more conventional approaches (IBS and FIR). In parallel to the growing number of studies validating EEG–fMRI findings with subsequent invasive electrophysiological recordings or post-operative follow-up, our information theoretic approach demonstrates that conventional approaches are adequate measures of epilepsy-related haemodynamic changes in the majority of cases. The clinical application of MI analysis *per se* would be particularly advised in patients with very frequent IED where a higher concern for inaccurate findings remains, due to deviations from linearity. In such case, MI might improve the delineation of the areas encoding the most epileptic information than linear methods (Nevado et al., 2004). Patient #2 exemplifies such situation and in this case MI, with its multidimensional representation, offered a more comprehensive understanding of the epileptic network.

Methodological considerations

In the current study, MI was computed based on the estimation of the entropy of the fMRI voxel time series as well as the entropy conditional to the EEG-score subsampled to the fMRI temporal resolution (EEG–fMRI score). Even though a binary discretization of the EEG-score was used in this work, the current methodology can easily be extended to consider more discrete bins in the EEG–fMRI score. If one ultimately considered computing the MI between the fMRI voxel time series and a "continuous" reference vector (e.g., the IED-informed BOLD regressor created by the convolution of the epileptic events with the HRF that is used in the GLM-based analysis), one might consider the estimation of the joint PDF, $p(X,Y)$, in addition to the marginal distributions, $p(X)$ and $p(Y)$ (Cover and Thomas, 1991). However, the number of samples required to obtain an accurate estimate of the joint PDF considerably increases resulting in computational inaccuracies, and more advanced methods to compute MI without first estimating the probability functions could be adopted (Gómez-Verdejo et al., 2012; Kraskov et al., 2004). Histograms of the PDFs were used to compute the plug-in MI values and the Panzeri–Treves procedure (Panzeri and Treves, 1996) was used to correct for the bias of the estimates due to the effect of limited sampling of the true PDFs. Equivalent results were also obtained by estimating the PDFs with kernel density estimators and then using these estimates to compute entropies and MI values (data not shown), corroborating the possibility of using alternative methods for calculating MI. This equivalence is particularly useful when applying bias correction approaches for simultaneous EEG and fMRI acquisitions because they have been mostly investigated with invasive electrophysiological data, such as single-unit recordings (Ince et al., 2012; Magri et al., 2012; Panzeri et al., 2007, 2008). An extension to our approach could also be to measure the (conditional) mutual information between single-trial features of the HRF (e.g. peak amplitude or time-to-peak), and the temporal or spectral features of the IED (e.g. amplitude at a certain lag, latency of first peak with respect to the IED onset, etc.). This information-theoretic evaluation will be carried out in future studies either at the electrode space (Ostwald et al., 2010) or the source (e.g. voxel-wise) space after computing the EEG inverse solution (Ostwald et al., 2011).

The number of ON time points in the EEG–fMRI score appears to be a relevant factor for the degree of concordance of the MI analysis. In general, the larger the number of ON time points in the EEG–fMRI score, the better the estimates of the probability density functions and MI are (Panzeri et al., 2007). On the one hand, the EEG–fMRI score presented less than 30 ON time points indicating the presence of epileptic activity in four discordant cases for MI (patients #3, #4, #7 and #9). Remarkably, both EEG–fMRI scores of patients #9 and #10 included 12 ON time points. Nevertheless, highly concordant clusters ($p<0.05$ NP-C) were revealed in patient #10, whereas discordant results were obtained in patient #9. This controversy may be explained in terms of the number of IED recorded during the acquisition (12 IED in patient #9, and 40 IED in patient #10 with several events during one TR) and the differences in the amplitude of the IED related BOLD signal changes at the latency of the maximum MI, which was about 10% in patient #10 whereas it was less than 1% in patient #9 (probably also due to arterio-venous malformation bleeding). On the other hand, the MI analysis in patients #10, #11 and #13 yielded highly concordant results with reduced statistical power in comparison with the GLM-based maps. This loss of power in the MI maps is in agreement with the fact that non-parametric approaches show less powerful results than equivalent parametric methods when the assumptions of the model are likely to be true (Nichols and Holmes, 2002) which is here confirmed by the high correspondence in the spatial localization of the clusters between the MI, FIR and IBS maps.

Finally, two out of the five discordant cases (patients #4 and #7) performed multiple large head jerks during the EEG–fMRI acquisition, whereas the discordant maps in patient #8 showed diffuse bilateral BOLD changes affecting all lobes suggestive for residual effects of head motion and cardiac-related artifacts (Vulliemoz et al., 2010b). In contrast to GLM-based approaches that enable the modeling of motion and physiological artifacts, our current information theoretic approach does not enable taking this information into account and future work will address this important methodological point for studies of epilepsy with EEG–fMRI (Lemieux et al., 2007; Liston et al., 2006; van Houdt et al., 2010a,b).

Conclusion

In summary, we proposed an information theoretic analysis based on mutual information between EEG and fMRI datasets in patients with focal epilepsy. Using this analysis framework we showed that the usual assumptions used in the conventional GLM analysis of spike-related BOLD changes (gaussianity, linearity, shape and latency of the HRF) are adequate although we obtained clinically more relevant results with MI in one case. In discordant cases, MI was generally not superior so that other sources of discrepancy must be studied. These results support the use of our analysis in candidates for epilepsy surgery in which decision making is difficult as the technique could improve confidence in more conventional BOLD findings. The potential role of MI for modeling the variability of the HRF as well as the use of other temporal or spectral features of the EEG and fMRI signals deserve further investigation in future studies.

Supplementary data to this article can be found online at http://dx.doi.org/10.1016/j.neuroimage.2012.12.011.

Acknowledgments

The authors want to thank the anonymous reviewers for their comments that helped to enhance the quality of the manuscript, and Prof. Panzeri for his guidance in the bias correction scheme. This work was supported in part by the Swiss National Science Foundation under grants 320030-122073, 320030-141165, 33CM30-140332 (SPUM Epilepsy) and PP00P2-123438, by the Medical Research Council under grant G0301067, and by the Center for Biomedical Imaging (CIBM) of the Universities and Hospitals of Geneva and Lausanne, and the EPFL.

References

Aghakhani, Y., Bagshaw, A.P., Bénar, C.G., Hawco, C., Andermann, F., Dubeau, F., Gotman, J., 2004. fMRI activation during spike and wave discharges in idiopathic generalized epilepsy. Brain 127 (Pt 5), 1127–1144.

Allen, P.J., Polizzi, G., Krakow, K., Fish, D.R., Lemieux, L., 1998. Identification of EEG events in the MR scanner: the problem of pulse artifact and a method for its subtraction. Neuroimage 8 (3), 229–239.

Allen, P.J., Josephs, O., Turner, R., 2000. A method for removing imaging artifact from continuous EEG recorded during functional MRI. Neuroimage 12 (2), 230–239.

Bagshaw, A.P., Aghakhani, Y., Bénar, C.G., Kobayashi, E., Hawco, C., Dubeau, F., Pike, G.B., Gotman, J., 2004. EEG–fMRI of focal epileptic spikes: analysis with multiple haemodynamic functions and comparison with gadolinium-enhanced MR angiograms. Hum. Brain Mapp. 22 (3), 179–192.

Bagshaw, A.P., Hawco, C., Bénar, C.G., Kobayashi, E., Aghakhani, Y., Dubeau, F., Pike, G.B., Gotman, J., 2005. Analysis of the EEG–fMRI response to prolonged bursts of interictal epileptiform activity. Neuroimage 24 (4), 1099–1112.
Bell, A.J., Sejnowski, T.J., 1995. An information-maximization approach to blind separation and blind deconvolution. Neural Comput. 7, 1129–1159.
Bénar, C.G., Gross, D.W., Wang, Y., Petre, V., Pike, B., Dubeau, F., Gotman, J., 2002. The BOLD response to interictal epileptiform discharges. Neuroimage 17 (3), 1182–1192.
Bénar, C.G., Grova, C., Kobayashi, E., Bagshaw, A.P., Aghakhani, Y., Dubeau, F., Gotman, J., 2006. EEG–fMRI of epileptic spikes: concordance with EEG source localisation and intracranial EEG. Neuroimage 30 (4), 1161–1170.
Buckner, R.L., Bandettini, P.A., O'Craven, K.M., Savoy, R.L., Petersen, S.E., Raichle, M.E., Rosen, B.R., 1996. Detection of cortical activation during averaged single trials of a cognitive task using functional magnetic resonance imaging. Proc. Natl. Acad. Sci. U. S. A. 93 (25), 14878–14883.
Caballero-Gaudes, C., 2010. Paradigm free mapping: detection and characterization of single trial fMRI BOLD responses without prior stimulus information. PhD thesis, University of Nottingham.
Caballero-Gaudes, C., Petridou, N., Francis, S.T., Dryden, I.L. and Gowland, P.A., in press. Paradigm free mapping with sparse regression automatically detects single-trial functional magnetic resonance imaging blood oxygenation level dependent responses. Hum. Brain Mapp. http://dx.doi.org/10.1002/hbm.21452.
Cover, T.M., Thomas, J.A., 1991. Elements of Information Theory. Wiley, New York.
Cox, R.W., 1996. AFNI: software for analysis and visualization of functional magnetic resonance neuroimages. Comput. Biomed. Res. 29 (3), 162–173.
Dale, A.M., Buckner, R.L., 1997. Selective averaging of rapidly presented individual trials using fMRI. Hum. Brain Mapp. 5 (5), 329–340.
de Zwart, J.A., van Gelderen, P., Jansma, J.M., Fukunaga, M., Bianciardi, M., Duyn, J.H., 2009. Hemodynamic nonlinearities affect BOLD fMRI response timing and amplitude. Neuroimage 47 (4), 1649–1658.
Disbrow, E.A., Slutsky, D.A., Roberts, T.P., Krubitzer, L.A., 2000. Functional MRI at 1.5 Tesla: a comparison of the blood oxygenation level-dependent signal and electrophysiology. Proc. Natl. Acad. Sci. U. S. A. 97 (17), 9718–9723.
Donaire, A., Bargallo, N., Falcón, C., Maestro, I., Carreno, M., Setoain, J., Rumià, J., Fernández, S., Pintor, L., Boget, T., 2009. Identifying the structures involved in seizure generation using sequential analysis of ictal-fMRI data. Neuroimage 47 (1), 173–183.
Friston, K.J., Fletcher, P., Josephs, O., Holmes, A., Rugg, M.D., Turner, R., 1998. Event-related fMRI: characterizing differential responses. Neuroimage 7 (1), 30–40.
Fuhrmann Alpert, G., Sun, F.T., Handwerker, D., D'Esposito, M., Knight, R.T., 2007. Spatio-temporal information analysis of event-related BOLD responses. Neuroimage 34 (4), 1545–1561.
Gómez-Verdejo, V., Martínez-Ramón, M., Florensa-Vila, J., Oliviero, A., 2012. Analysis of fMRI time series with mutual information. Med. Image Anal. 16 (2), 451–458.
Gotman, J., 2008. Epileptic networks studied with EEG–fMRI. Epilepsia 49 (Suppl. 3), 42–51.
Gotman, J., Pittau, F., 2011. Combining EEG and fMRI in the study of epileptic discharges. Epilepsia 52 (Suppl. 4), 38–42.
Gotman, J., Grova, C., Bagshaw, A., Kobayashi, E., Aghakhani, Y., Dubeau, F., 2005. Generalized epileptic discharges show thalamocortical activation and suspension of the default state of the brain. Proc. Natl. Acad. Sci. U. S. A. 102 (42), 15236–15240.
Grouiller, F., Vercueil, L., Krainik, A., Segebarth, C., Kahane, P., David, O., 2010. Characterization of the hemodynamic modes associated with interictal epileptic activity using a deformable model-based analysis of combined EEG and functional MRI recordings. Hum. Brain Mapp. 31 (8), 1157–1173.
Grouiller, F., Thornton, R.C., Groening, K., Spinelli, L., Duncan, J.S., Schaller, K., Siniatchkin, M., Lemieux, L., Seeck, M., Michel, C.M., Vulliemoz, S., 2011. With or without spikes: localisation of focal epileptic activity by simultaneous electroencephalography and functional magnetic resonance imaging. Brain 134 (Pt 10), 2867–2886.
Hamandi, K., Salek-Haddadi, A., Liston, A., Laufs, H., Fish, D.R., Lemieux, L., 2005. fMRI temporal clustering analysis in patients with frequent interictal epileptiform discharges: comparison with EEG-driven analysis. Neuroimage 26 (1), 309–316.
Hamandi, K., Salek-Haddadi, A., Laufs, H., Liston, A., Friston, K., Fish, D.R., Duncan, J.S., Lemieux, L., 2006. EEG–fMRI of idiopathic and secondarily generalized epilepsies. Neuroimage 31 (4), 1700–1710.
Hawco, C.S., Bagshaw, A.P., Lu, Y., Dubeau, F., Gotman, J., 2007. BOLD changes occur prior to epileptic spikes seen on scalp EEG. Neuroimage 35 (4), 1450–1458.
Heckman, G.M., Bouvier, S.E., Carr, V.A., Harley, E.M., Cardinal, K.S., Engel, S.A., 2007. Nonlinearities in rapid event-related fMRI explained by stimulus scaling. Neuroimage 34 (2), 651–660.
Hlinka, J., Palus, M., Vejmelka, M., Mantini, D., Corbetta, M., 2011. Functional connectivity in resting-state fMRI: is linear correlation sufficient? Neuroimage 54 (3), 2218–2225.
Ince, R.A., Mazzoni, A., Bartels, A., Logothetis, N.K., Panzeri, S., 2012. A novel test to determine the significance of neural selectivity to single and multiple potentially correlated stimulus features. J. Neurosci. Methods 210 (1), 49–65.
Iriarte, J., Urrestarazu, E., Artieda, J., Valencia, M., LeVan, P., Viteri, C., Alegre, M., 2006. Independent component analysis in the study of focal seizures. J. Clin. Neurophysiol. 23 (6), 551–558.
Jacobs, J., Kobayashi, E., Boor, R., Muhle, H., Stephan, W., Hawco, C., Dubeau, F., Jansen, O., Stephani, U., Gotman, J., Siniatchkin, M., 2007. Hemodynamic responses to interictal epileptiform discharges in children with symptomatic epilepsy. Epilepsia 48 (11), 2068–2078.
Jacobs, J., Hawco, C., Kobayashi, E., Boor, R., LeVan, P., Stephani, U., Siniatchkin, M., Gotman, J., 2008. Variability of the hemodynamic response as a function of age and frequency of epileptic discharge in children with epilepsy. Neuroimage 40 (2), 601–614.
Jacobs, J., Levan, P., Moeller, F., Boor, R., Stephani, U., Gotman, J., Siniatchkin, M., 2009. Hemodynamic changes preceding the interictal EEG spike in patients with focal epilepsy investigated using simultaneous EEG–fMRI. Neuroimage 45 (4), 1220–1231.
Jann, K., Wiest, R., Hauf, M., Meyer, K., Boesch, C., Mathis, J., Schroth, G., Dierks, T., Koenig, T., 2008. BOLD correlates of continuously fluctuating epileptic activity isolated by independent component analysis. Neuroimage 42 (2), 635–648.
Khalidov, I., Fadili, M.J., Lazeyras, F., Van de Ville, D., Unser, M., 2011. Activelets: Wavelets for sparse representation of hemodynamic responses. Signal Process. 91 (12), 2810–2821.
Khatamian, Y.B., Fahoum, F., Gotman, J., 2011. Limits of 2D-TCA in detecting BOLD responses to epileptic activity. Epilepsy Res. 94 (3), 177–188.
Kobayashi, E., Bagshaw, A.P., Grova, C., Dubeau, F., Gotman, J., 2006. Negative BOLD responses to epileptic spikes. Hum. Brain Mapp. 27 (6), 488–497.
Kraskov, A., Stögbaurer, H., Grassberger, P., 2004. Estimating mutual information. Phys. Rev. E 69 (6), 066138.
Laufs, H., Hamandi, K., Salek-Haddadi, A., Kleinschmidt, A.K., Duncan, J.S., Lemieux, L., 2007. Temporal lobe interictal epileptic discharges affect cerebral activity in "default mode" brain regions. Hum. Brain Mapp. 28 (10), 1023–1032.
Lazeyras, F., Blanke, O., Perrig, S., Zimine, I., Golay, X., Delavelle, J., Michel, C.M., de Tribolet, N., Villemure, J.G., Seeck, M., 2000. EEG-triggered functional MRI in patients with pharmacoresistant epilepsy. J. Magn. Reson. Imaging 12 (1), 177–185.
Lemieux, L., Salek-Haddadi, A., Lund, T.E., Laufs, H., Carmichael, D., 2007. Modelling large motion events in fMRI studies of patients with epilepsy. Magn. Reson. Imaging 25 (6), 894–901.
Lemieux, L., Laufs, H., Carmichael, D., Paul, J.S., Walker, M.C., Duncan, J.S., 2008. Noncanonical spike-related BOLD responses in focal epilepsy. Hum. Brain Mapp. 29 (3), 329–345.
LeVan, P., Tyvaert, L., Gotman, J., 2010a. Modulation by EEG features of BOLD responses to interictal epileptiform discharges. Neuroimage 50 (1), 15–26.
LeVan, P., Tyvaert, L., Moeller, F., Gotman, J., 2010b. Independent component analysis reveals dynamic ictal BOLD responses in EEG–fMRI data from focal epilepsy patients. Neuroimage 49 (1), 366–378.
Liston, A.D., Lund, T.E., Salek-Haddadi, A., Hamandi, K., Friston, K.J., Lemieux, L., 2006. Modelling cardiac signal as a confound in EEG–fMRI and its application in focal epilepsy studies. Neuroimage 30 (3), 827–834.
Liu, Z., Rios, C., Zhang, N., Yang, L., Chen, W., He, B., 2010. Linear and nonlinear relationships between visual stimuli, EEG and BOLD fMRI signals. Neuroimage 50 (3), 1054–1066.
Lizier, J.T., Heinzle, J., Horstmann, A., Haynes, J.D., Prokopenko, M., 2010. Multivariate information-theoretic measures reveal directed information structure and task relevant changes in fMRI connectivity. J. Comput. Neurosci. 30 (1), 85–107.
Lopes, R., Lina, J.M., Fahoum, F., Gotman, J., 2012. Detection of epileptic activity in fMRI without recording the EEG. Neuroimage 60 (3), 1867–1879.
Lu, Y., Bagshaw, A.P., Grova, C., Kobayashi, E., Dubeau, F., Gotman, J., 2006. Using voxel-specific hemodynamic response function in EEG–fMRI data analysis. Neuroimage 32 (1), 238–247.
Lu, Y., Grova, C., Kobayashi, E., Dubeau, F., Gotman, J., 2007. Using voxel-specific hemodynamic response function in EEG–fMRI data analysis: An estimation and detection model. Neuroimage 34 (1), 195–203.
Magri, C., Whittingstall, K., Singh, V., Logothetis, N.K., Panzeri, S., 2009. A toolbox for the fast information analysis of multiple-site LFP, EEG and spike train recordings. BMC Neurosci. 10 (1), 81.
Magri, C., Schridde, U., Murayama, Y., Panzeri, S., Logothetis, N.K., 2012. The amplitude and timing of the BOLD signal reflects the relationship between local field potential power at different frequencies. J. Neurosci. 32 (4), 1395–1407.
Marques, J.P., Rebola, J., Figueiredo, P., Pinto, A., Sales, F., Castelo-Branco, M., 2009. ICA decomposition of EEG signal for fMRI processing in epilepsy. Hum. Brain Mapp. 30 (9), 2986–2996.
Mirsattari, S.M., Wang, Z., Ives, J.R., Bihari, F., Leung, L.S., Bartha, R., Menon, R.S., 2006. Linear aspects of transformation from interictal epileptic discharges to BOLD fMRI signals in an animal model of occipital epilepsy. Neuroimage 30 (4), 1133–1148.
Moeller, F., LeVan, P., Gotman, J., 2011. Independent component analysis (ICA) of generalized spike wave discharges in fMRI: comparison with general linear model-based EEG–fMRI. Hum. Brain Mapp. 32 (2), 209–217.
Morgan, V.L., Price, R.R., Arain, A., Modur, P., Abou-Khalil, B., 2004. Resting functional MRI with temporal clustering analysis for localisation of epileptic activity without EEG. Neuroimage 21 (1), 473–481.
Morgan, V.L., Li, Y., Abou-Khalil, B., Gore, J.C., 2008. Development of 2dTCA for the detection of irregular, transient BOLD activity. Hum. Brain Mapp. 29 (1), 57–69.
Nevado, A., Young, M.P., Panzeri, S., 2004. Functional imaging and neural information coding. Neuroimage 21 (3), 1083–1095.
Nichols, T.E., Holmes, A.P., 2002. Nonparametric permutation tests for functional neuroimaging: a primer with examples. Hum. Brain Mapp. 15 (1), 1–25.
Ostwald, D., Bagshaw, A.P., 2011. Information theoretic approaches to functional neuroimaging. Magn. Reson. Imaging 29 (10), 1417–1428.
Ostwald, D., Porcaro, C., Bagshaw, A.P., 2010. An information theoretic approach to EEG–fMRI integration of visually evoked responses. Neuroimage 49 (1), 498–516.
Ostwald, D., Porcaro, C., Bagshaw, A.P., 2011. Voxel-wise information theoretic EEG–fMRI feature integration. Neuroimage 55 (3), 1270–1286.
Ostwald, D., Porcaro, C., Mayhew, S.D., Bagshaw, A.P., 2012. EEG–fMRI based information theoretic characterization of the human perceptual decision system. PLoS One 7 (4), e33896.
Panzeri, S., Treves, A., 1996. Analytical estimates of limited sampling biases in different information measures. Netw. Comput. Neural Syst. 7, 87–107.
Panzeri, S., Senatore, R., Montemurro, M.A., Petersen, R.S., 2007. Correcting for the sampling bias problem in spike train information measures. J. Neurophysiol. 98 (3), 1064–1072.
Panzeri, S., Magri, C., Logothetis, N.K., 2008. On the use of information theory for the analysis of the relationship between neural and imaging signals. Magn. Reson. Imaging 26 (7), 1015–1025.

Patel, R.S., Van De Ville, D., Bowman, F.D., 2006. Determining significant connectivity by 4D spatiotemporal wavelet packet resampling of functional neuroimaging data. Neuroimage 31 (3), 1142–1155.
Pittau, F., Levan, P., Moeller, F., Gholipour, T., Haegelen, C., Zelmann, R., Dubeau, F., Gotman, J., 2011. Changes preceding interictal epileptic EEG abnormalities: comparison between EEG/fMRI and intracerebral EEG. Epilepsia 52 (6), 1120–1129.
Raichle, M.E., MacLeod, A.M., Snyder, A.Z., Powers, W.J., Gusnard, D.A., Shulman, G.L., 2001. A default mode of brain function. Proc. Natl. Acad. Sci. U. S. A. 98 (2), 676–682.
Rathakrishnan, R., Moeller, F., Levan, P., Dubeau, F., Gotman, J., 2010. BOLD signal changes preceding negative responses in EEG–fMRI in patients with focal epilepsy. Epilepsia 51 (9), 1837–1845.
Rodionov, R., De Martino, F., Laufs, H., Carmichael, D.W., Formisano, E., Walker, M., Duncan, J.S., Lemieux, L., 2007. Independent component analysis of interictal fMRI in focal epilepsy: comparison with general linear model-based EEG-correlated fMRI. Neuroimage 38 (3), 488–500.
Saad, Z.S., Glen, D.R., Chen, G., Beauchamp, M.S., Desai, R., Cox, R.W., 2009. A new method for improving functional-to-structural MRI alignment using local Pearson correlation. Neuroimage 44 (3), 839–848.
Salek-Haddadi, A., Diehl, B., Hamandi, K., Merschhemke, M., Liston, A., Friston, K., Duncan, J.S., Fish, D.R., Lemieux, L., 2006. Hemodynamic correlates of epileptiform discharges: an EEG–fMRI study of 63 patients with focal epilepsy. Brain Res. 1088 (1), 148–166.
Schwartz, T.H., Hong, S.B., Bagshaw, A.P., Chauvel, P., Bénar, C.G., 2011. Preictal changes in cerebral haemodynamics: review of findings and insights from intracerebral EEG. Epilepsy Res. 97 (3), 252–266.
Shannon, C.E., 1948. A mathematical theory of communication. Bell Syst. Tech. J. 27, 623–656.
Thornton, R.C., Rodionov, R., Laufs, H., Vulliemoz, S., Vaudano, A., Charmichael, D., Cannadathu, S., Guye, M., McEvoy, A., Lhatoo, S., Bartolomei, F., Chauvel, P., Diehl, B., De Martino, F., Elwes, R.D., Walker, M.C., Duncan, J.S., Lemieux, L., 2010a. Imaging haemodynamic changes related to seizures: comparison of EEG-based general linear model, independent component analysis of fMRI and intracranial EEG. Neuroimage 53 (1), 196–205.
Thornton, R., Laufs, H., Rodionov, R., Cannadathu, S., Carmichael, D.W., Vulliemoz, S., Salek-Haddadi, A., McEvoy, A.W., Smith, S.M., Lhatoo, S., Elwes, R.D., Guye, M., Walker, M.C., Lemieux, L., Duncan, J.S., 2010b. EEG correlated functional MRI and postoperative outcome in focal epilepsy. J. Neurol. Neurosurg. Psychiatry 81 (8), 922–927.
Thornton, R., Vulliemoz, S., Rodionov, R., Carmichael, D.W., Chaudhary, U.J., Diehl, B., Laufs, H., Vollmar, C., McEvoy, A.W., Walker, M.C., Bartolomei, F., Guye, M., Chauvel, P., Duncan, J.S., Lemieux, L., 2011. Epileptic networks in focal cortical dysplasia revealed using electroencephalography-functional magnetic resonance imaging. Ann Neurol. 70 (5), 822–837.
Tyvaert, L., LeVan, P., Dubeau, F., Gotman, J., 2009. Noninvasive dynamic imaging of seizures in epileptic patients. Hum. Brain Mapp. 30 (12), 3993–4011.
van Houdt, P.J., de Munck, J.C., Zijlmans, M., Huiskamp, G., Leijten, F.S., Boon, P.A., Ossenblok, P.P., 2010a. Comparison of analytical strategies for EEG-correlated fMRI data in patients with epilepsy. Magn. Reson. Imaging 28 (8), 1078–1086.
van Houdt, P.J., Ossenblok, P.P., Boon, P.A., Leijten, F.S., Velis, D.N., Stam, C.J., de Munck, J.C., 2010b. Correction for pulse height variability reduces physiological noise in functional MRI when studying spontaneous brain activity. Hum. Brain Mapp. 31 (2), 311–325.
Vanzetta, I., Flynn, C., Ivanov, A.I., Bernard, C., Bénar, C.G., 2010. Investigation of linear coupling between single-event blood flow responses and interictal discharges in a model of experimental epilepsy. J. Neurophysiol. 103 (6), 3139–3152.
Voges, N., Blanchard, S., Wendling, F., David, O., Benali, H., Papadopoulo, T., Clerc, M., Bénar, C., 2012. Modelling of the neurovascular coupling in epileptic discharges. Brain Topogr. 25 (2), 136–156.
Vulliemoz, S., Thornton, R., Rodionov, R., Carmichael, D.W., Guye, M., Lhatoo, S., McEvoy, A.W., Spinelli, L., Michel, C.M., Duncan, J.S., Lemieux, L., 2009. The spatio-temporal mapping of epileptic networks: combination of EEG–fMRI and EEG source imaging. Neuroimage 46 (3), 834–843.
Vulliemoz, S., Lemieux, L., Daunizeau, J., Michel, C.M., Duncan, J.S., 2010a. The combination of EEG source imaging and EEG-correlated functional MRI to map epileptic networks. Epilepsia 51 (4), 491–505.
Vulliemoz, S., Rodionov, R., Carmichael, D.W., Thornton, R., Guye, M., Lhatoo, S.D., Michel, C.M., Duncan, J.S., Lemieux, L., 2010b. Continuous EEG source imaging enhances analysis of EEG–fMRI in focal epilepsy. Neuroimage 49 (4), 3219–3229.
Vulliemoz, S., Carmichael, D.W., Rosenkranz, K., Diehl, B., Rodionov, R., Walker, M.C., McEvoy, A.W., Lemieux, L., 2011. Simultaneous intracranial EEG and fMRI of interictal epileptic discharges in humans. Neuroimage 54 (1), 182–190.
Windischberger, C., Cunnington, R., Lamm, C., Lanzenberger, R., Langenberger, H., Deecke, L., Bauer, H., Moser, E., 2008. Time-resolved analysis of fMRI signal changes using Brain Activation Movies. J. Neurosci. Methods 169 (1), 222–230.
Zijlmans, M., Huiskamp, G., Hersevoort, M., Seppenwoolde, J.H., van Huffelen, A.C., Leijten, F.S., 2007. EEG–fMRI in the preoperative work-up for epilepsy surgery. Brain 130 (Pt 9), 2343–2353.